Emission Line Imaging Spectroscopy for Diagnosing of Solar Outer Atmospheres

Tetsuya WATANABE and the EIS Team
National Astronomical Observatory, Japan

(Received 18 January 2007 / Accepted 16 April 2007)

The Extreme Ultraviolet Imaging Spectrometer on board the Japanese Sun Observing Satellite "*Hinode*" realizes the highest sensitivity ever achieved in the two EUV wavelengths of 17-21 nm and 25-29 nm. EIS will be able to provide the detailed diagnostic information on solar corona and transition region. A new tool of time-dependent collisonal-radiative model will be developed to analyze the data taken by this EIS instrument, and to diagnose temperatures and densities of those plasmas in the outer atmospheres of the Sun.

Keywords: Hinode mission, solar corona, solar transition region, coronal heating, EUV spectroscopy

DOI: 10.1585/pfr.2.S1011

1. Introduction

A Japanese Sun Observing Satellite, *Hinode* was launched on 23-Sep-2006. The EUV imaging spectrometer (EIS) on board *Hinode* accommodates the multilayer coated mirror and concave grating with back-illuminated CCDs for detectors, and realizes the highest sensitivity ever achieved in the two EUV wavelengths, i.e. 17-21 nm and 25-29 nm. Thanks to the normal incidence optics, the flexibility of designing the spectrograph and the grating were best optimized to obtain excellent imaging capability. The instrument was designed, fabricated, and tested by an international consortium, consisting of NAOJ, JAXA (Japan); MSSL, RAL, and UB (UK); NASA and NRL (USA); and UO (Norway).

The scientific goals of the instruments on board are: a) to identify the mechanisms responsible for heating the corona in active regions and the quiet Sun, b) to establish the mechanisms that give rise to transient phenomena, such as flares and coronal mass ejections, and c) to investigate the processes responsible for energy transfer from the photosphere to the corona. The instrument EIS will be able to provide the detailed diagnostic information on solar corona and transition region [1].

After opening of the instrument doors, the first light of EIS took place successfully on 28-Oct-2006. Functions for scientific observations were verified during the commissioning phase in November and the period of the initial 90 day scientific observation started at the beginning of December. So far, all parts of the EIS instrument are performing properly, as tested before the launch.

In this paper, we are just going to demonstrate the on board performance of the instrument after the first light.

author's e-mail: watanabe@uvlab.mtk.nao.ac.jp

2. Instrumentation

The major improvement of the EIS telescope throughput was achieved by applying the multi-layer coatings to the mirror and the grating used in the EUV wavelengths of 50-500 Å. These processes, of course, rather restrict the free spectral ranges of the optical elements in EUV, but the improvement of reflectivity in the tuned wavelengths receives more merit than those without. The parameters of the instrument are summarized in Table 1. The optical lay-

Table 1 EIS parameters.

Wavelength Bands	170-190 Å & 250-290 Å
Peak Effective Areas	0.30 cm^2 & 0.11 cm^2
Primary Mirror	15 cm diameter, two Mo/Si multilayer coating
Grating	Toroidal & laminar, 4200 grooves·mm^{-1}, two Mo/Si multilayer coating
CCD Cameras	Two back-thinned E2V CCDs, $2048 \times 1024 \times 13.5$ μm pix.
Plate Scales	13.53 μm/arcsec at CCD; 9.40 μm/arcsec at slit
Spatial Resolution (pix)	2 arcsec (1 arcsec)
Field of View	6 arcmin $\times$ 8.5 arcmin
Raster	1 arcsec in 0.7 sec, min. step 0.123 arcsec
Slit/Slot Widths	1, 2, 40, & 266 arcsec
Spectral Resolution	47 mÅ (FWHM) at 185 Å; 1 pix = 22 mÅ, approx. 25 km s^{-1}/pix
Temperature Coverage	$\log T = 4.7$-7.3 K
CCD Frame Read Time	0.8 sec
Line Observation	Simultaneous observation of up to 25 lines

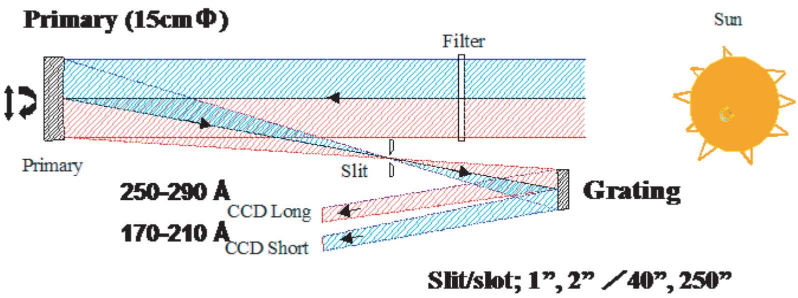

Fig. 1 Optical layout of EIS.

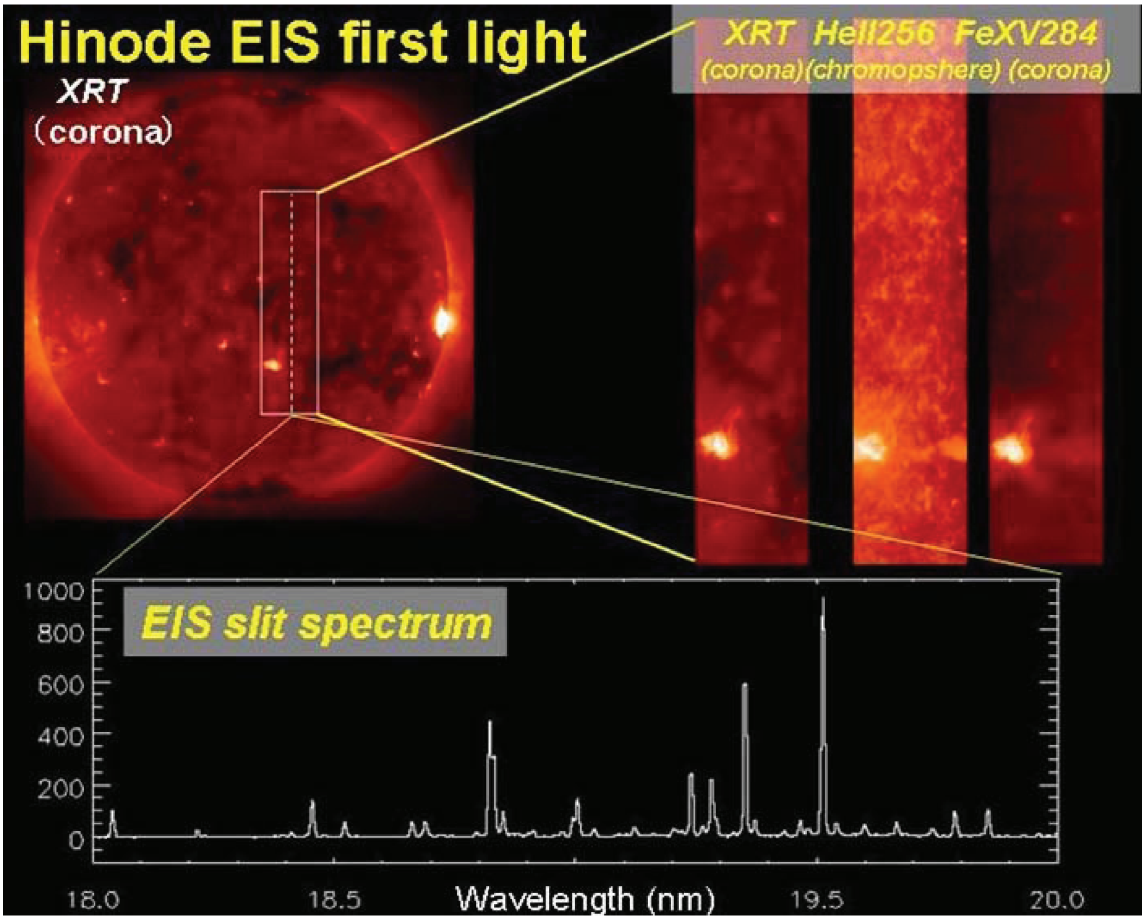

Fig. 2 First Light of EIS (28-Oct-06): In the top left panel, a white square shows the location of the 40 arcsec slot on the solar X-ray image taken by XRT. Three right panels are the images in this FOV, of XRT, HeIIλ256Å, and FeXVλ284Å. The bottom panel is a spectrum taken along a dotted line on the solar surface with the 1 arcsec slit.

out is shown in Fig. 1. The EIS instrument has only two reflections, the mirror and the concave grating with multilayer coatings, so that the throughput of the telescope is designed to achieve the highest sensitivity among the instruments ever flown, aiming to observe in the same wavelengths. The plate scale that 1 pixel size on the CCD detectors corresponds to 1 arcsec means that the pixel spectral resolution is 0.00223 Å. The simulation tells that we can determine the line center location and width of spectral lines with an accuracy of 1 km s^{-1} and 3 km s^{-1}, respectively. Slot images (overlappograms) provide spatial emission line intensity distribution on the Sun, as the Sun emits mostly in emission lines, although spectral information is folded on the images.

3. First Light

The doors of the clamshell, an equipment to protect thin metal filters from the M-V rocket launching environment, accommodated at the aperture, were opened on 27 and 28 of October, 2006, more than a month after the launch, as the EUV instruments have to avoid the contamination of particles and organic material.

Figure 2 shows the first light images of EIS released to the open public on 31-Oct-06. The fields of view of

EIS on the solar surface were indicated on the image of X-Ray Telescope (XRT) on board *Hinode*. Slot images of HeIIλ256 Å and FeXVλ284 Å were shown on the right hand chart of Fig. 2. The helium line is formed in the upper chromosphere, and its slot image clearly shows chromospheric network structures, while the right most iron line image shows typical coronal structures, such as active-region coronal loops and tiny X-ray bright points, and they are very similar to the X-ray image taken by XRT. An arcsec narrow slit was put on the quiet-sun region the same day. A spectrum in the wavelengths $\lambda\lambda$180-200 Å is shown at the bottom of Fig. 2. In the spectrum, strong iron emission lines at various ionization stages from FeVIII to FeXVII can be detected. Spectral shapes as well as counting rates of these lines shows that the performance of the instrument on board is as we expected on the ground before the launch; Fig. 3 is a comparison of the observed spectra with the simulation code, CHIANTI [4], multiplied by the EIS throughput.

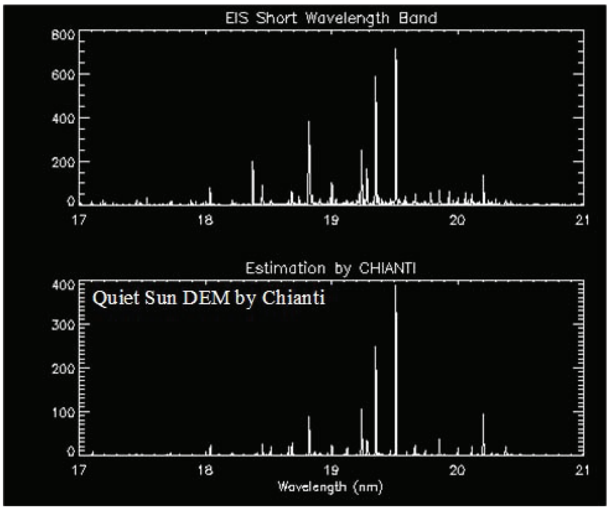

Fig. 3 Comparison with CHIANTI, a spectrum simulating code for astrophysical plasmas [4] for the EIS short wavelength band.

4. Superior Image and Spectral Quality

In the field of solar EUV spectroscopic researches, EIS on board the *Hinode* was the first satellite born telescope that accommodates a normal incidence optical system. On the *SoHO* spacecraft, the Coronal Diagnostic Spectrometer (CD) is an instrument observing solar EUV emission lines. It is a Walter Type-II grazing telescope taking spectra with a normal incidence spectrograph (NIS) of low spectral resolution and a grazing incidence spectrograph (GIS) for rather a high sensitivity slot (2 arcsec × 2 arcsec) observation. The former has a CCD camera as its detector, while the latter has a position sensitive proportional counter.

Figure 4 compares image quality of CDS/NIS and EIS

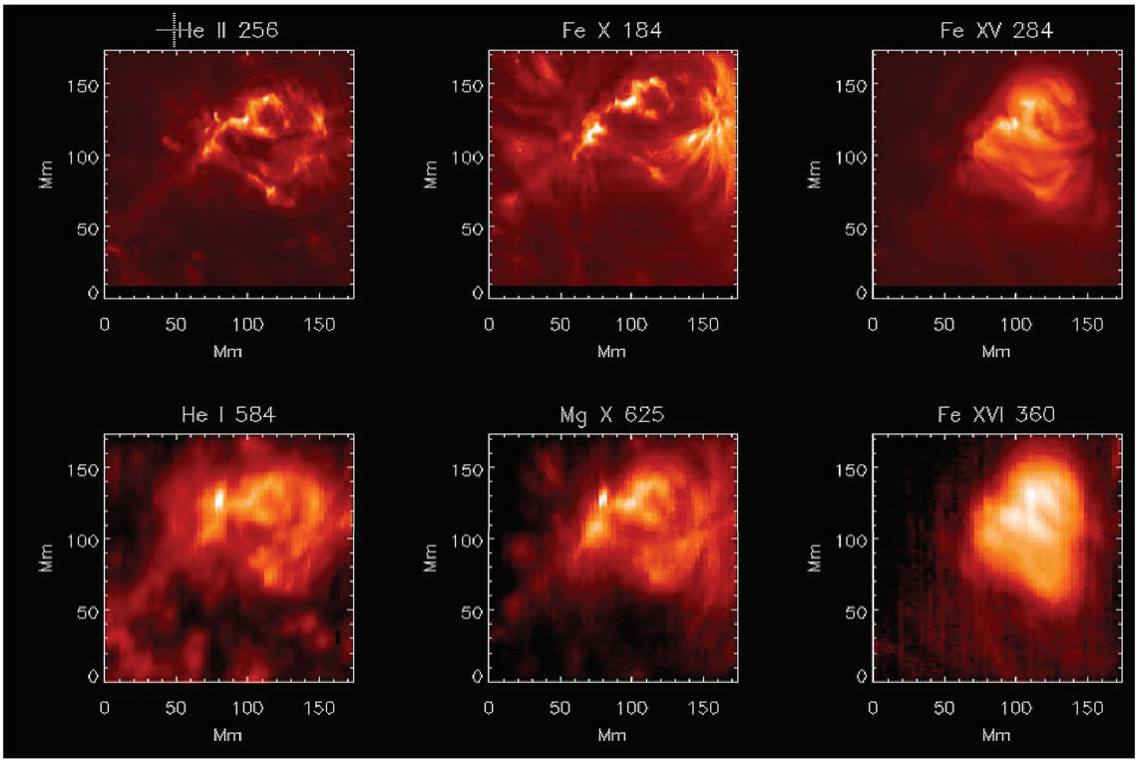

Fig. 4 Improved Image Quality (Comparison with CDS/NIS): Top panels are EIS raster images of HII (chromosphere), FeX (low-temperature corona), and FeXV (high-temperature corona) lines, and bottom panels show corresponding temperature images of HeI, MgX, and FeXVI lines observed by CDS.

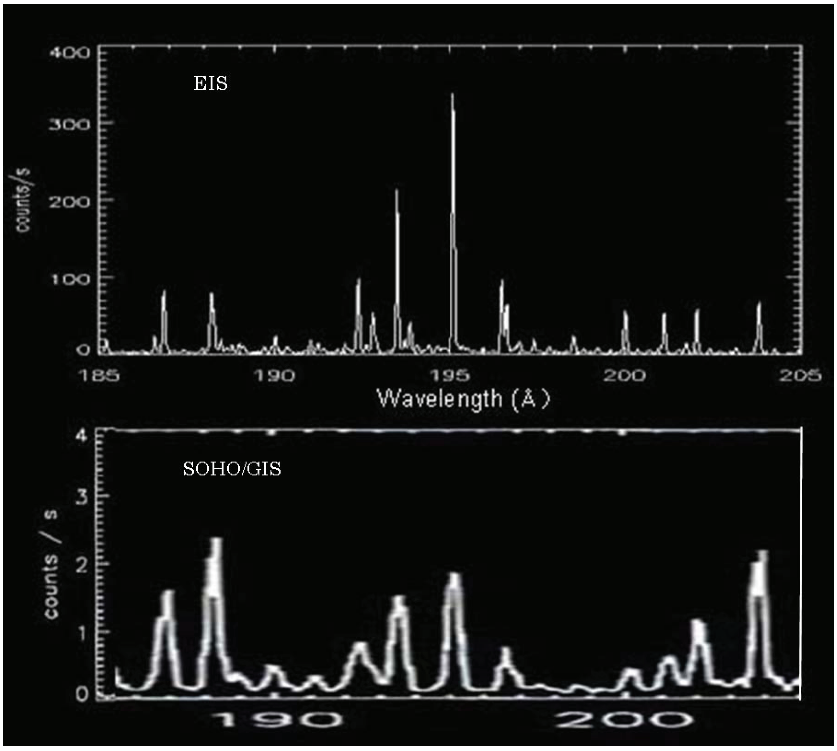

Fig. 5 Improved image quality (comparison with CDS/GIS).

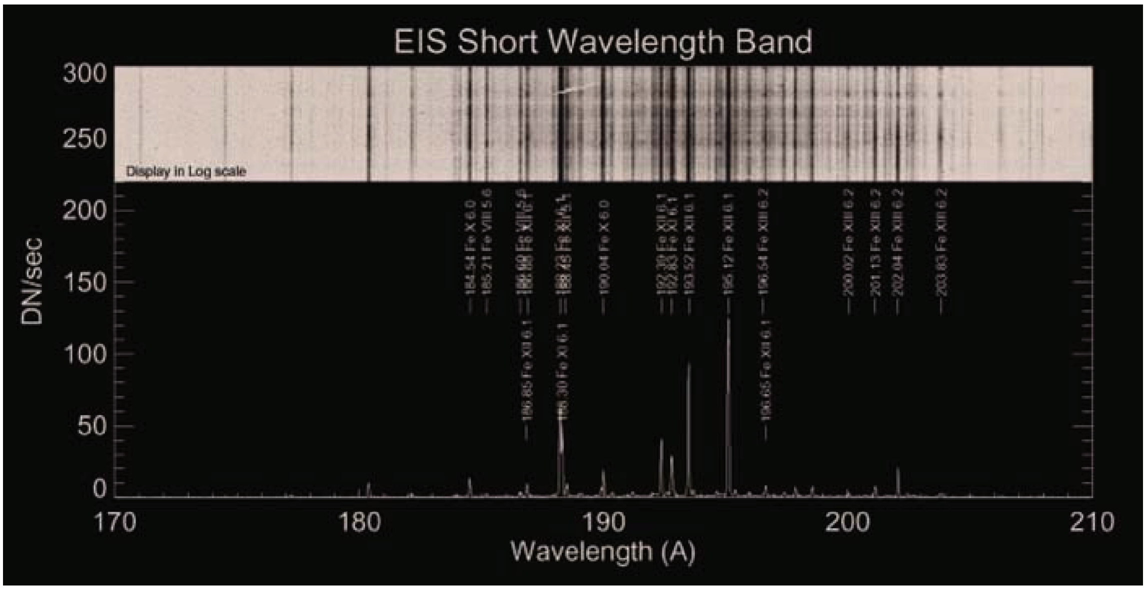

Fig. 6 EIS short wavelength spectrum.

in various emission lines. The active region AR10923 was nearly simultaneously observed by the both space born instruments in November 2006. Here are HeI and HeII lines of chromospheric or lower transition-region origin, FeX and MgX lines for low coronal temperatures, and FeXV and XVI lines are from higher temperature corona in Fig. 4. In all the temperature ranges, the improvement of spatial resolution is significant, perhaps EIS has about three-times better spatial resolution than that of CDS/NIS, although we have to wait for the report of more accurate on board calibration. Figure 5 shows the improvement of spectral resolution. The short wavelengths of EIS observing band are only observed by CDS/GIS. As the result, both spectral resolution and sensitivity of the EIS spectrograph is very much improved from those of the predecessor's capability.

Table 2 Density sensitive line ratios for EIS observation.

ION	LOG TEMPERATURE (K)	RATIO (Å/Å)	LOG N_E-RANGE (CM^{-3})
SiX	6.1	258.4/261.0	8.0 – 10.0
SX	6.1	196.8/264.2	8.0 – 12.0
FeXII	6.1	186.9/195.1	8.0 – 12.0
FeXIII	6.2	203.8/202.0	8.5 – 10.5
SXI	6.3	285.8/281.4	8.0 – 10.0
		190.4/191.3	10.5 – 12.5
FeXIX	6.3	264.8/274.2	9.0 – 11.0
NiXVI	6.4	194.0/185.2	9.5 – 11.5
ArXIV	6.5	188.0/199.4	10.0 – 12.0

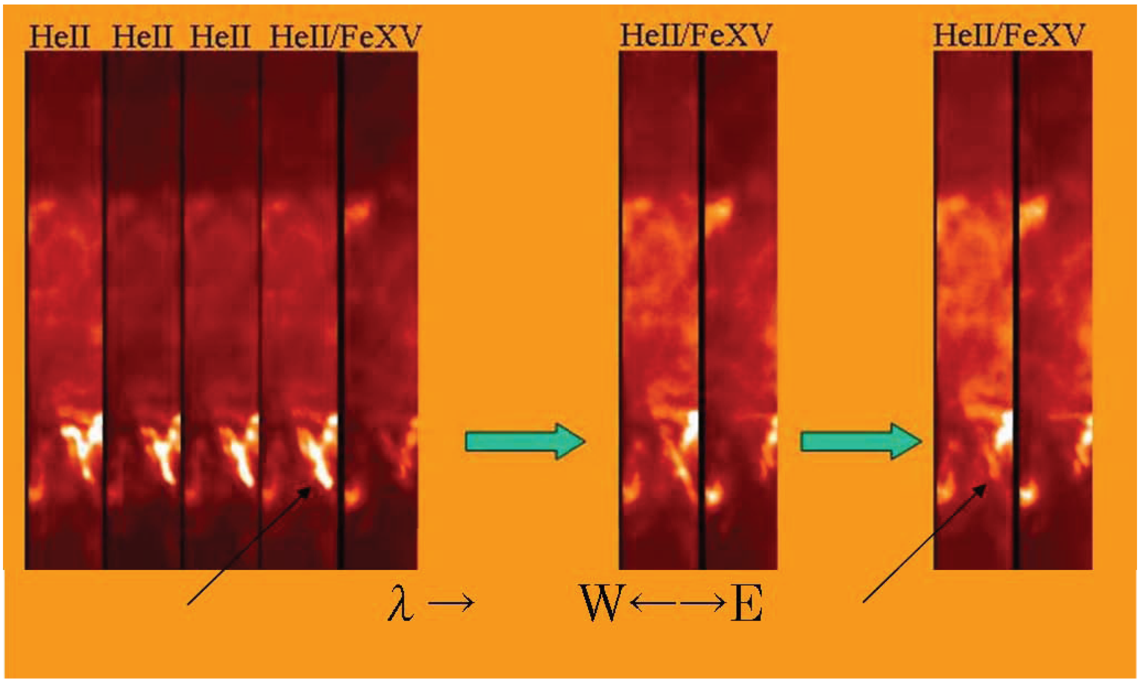

Fig. 7 An EUV jet associated with the active region AR10923: First four images show the evolution of a jet seen in HeII images till its intensity maximum. Three sets of simultaneously taken HeII and FeXV images during the decay phase of the jet. Arrows indicate a dog-legged structure combining an angular magnetic configuration with a change of jet velocities in various temperatures.

5. Spectral Line Identification

Thanks to the ever best performance achieved by the solar EUV instruments, a large number of emission lines are detected in EIS spectra. Figure 6 is just an example of 10 second exposure time spectrum in the shorter observing wavelength of EIS taken on 28-Nov-2006, the very first day of EIS observation. The wavelength is rich of iron emission lines at various ionization stages; namely, from FeVIII to FeXVII M-shell transitions. Once a flare occurs and the plasma heating takes place, the resonance lines of iron lithium-like ion (FeXXIV) will be observed in the both short and long EIS observing wavelengths, as well as FeXXIII lines used for temperature diagnostics.

Several line pairs shown in Table 2 will give information on electron density in the solar corona. A tentative line ratio analysis of FeXIII of 202.0 Å/203.8 Å pair shows a clear evidence for density changes from the quiet-sun to active region, from $10^{8.5}$-10^{10} cm^{-3}.

6. Dynamic Changes of Solar Outer Atmospheres

Solar outer atmospheres are always very dynamic, and this is why we need a fast telescope in every wavelength for observation. Nevertheless, no solar EUV spectrographs had a chance to make an exposure time of order of a second. Thanks to the improvement of sensitivity, EIS will be the first instrument to make such observations in the solar transition region and corona.

The slot observation, taking “overlappograms” will be one of capable tools to catch such rapidly changing phenomena taking place on the solar surface. An example is shown in Fig. 7, showing the outbreak of an EUV jet.

In Fig. 7 only HeII256 Å and FeXV284 Å line over-

Table 3 Relaxation time scales by Brooks and Summers [5].

	$N_e(cm^{-3})$	$T_e(K)$	$\tau_{transient}$
upper chromosphere	3.7×10^{10}	2×10^4	$\sim 5 \rightarrow 6$ minutes
transition region	$1.3 \times 10^{10} \rightarrow 1.3 \times 10^9$	$5 \times 10^4 \rightarrow 5 \times 10^5$	$\sim 3 \rightarrow 20$ min utes
corona	5.4×10^8	1×10^6	~ 1 hour

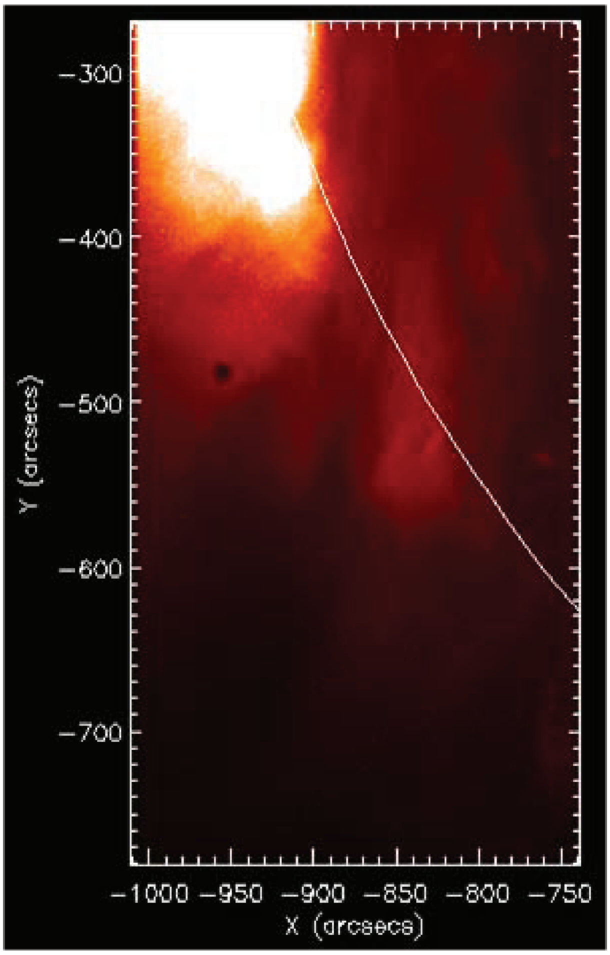

Fig. 8 Mercury transit seen by EIS.

lappograms are shown, though images of nine coronal lines are available. In this observation, the cadence is moderate and the overlappograms are taken every 30 seconds. It is easily noticed that the contrast of the jet reveals completely different features in the chromospheric line and coronal line. During the uprising phase, both lines appears in emission, and HeII features show complicated structures, perhaps coming from both dog-legged magnetic configuration and chromospheric velocity distribution coupled in the overlappogram. During the decay phase, FeXV becomes faint faster or a sort of absorption appears, showing rapid cooling takes place in the coronal temperature.

Numerous active phenomena take place not only in active regions but also in quiet-sun regions, such as transient brightenings, explosive events, blinkers, etc. Further to understand the physics of these phenomena, fast cadence EIS observations with slot and slit rastering with limited fields of view will be very important.

7. Mercury Transit (8-Nov-2006)

Mercury passed in front of the solar disk on 8-Nov-2006 (see Fig. 8), and the *Hinode* telescopes tracked the whole process. This phenomenon is used to confirm the performance of the telescope and to know the misalignment of the three telescopes on board. The analysis of the latter is on the way.

8. Tool for Analyzing Non-Equilibrium Plasmas

Solar outer atmospheres are very dynamic, and plasma temperatures change roughly two orders of magnitudes from chromosphere to corona in just a few hundred kilometers.

Table 3 indicates that solar chromospheric and coronal plasmas need a few minutes or more to reach the ionization equilibrium. If so, all the phenomena seen by EIS in the EUV wavelengths should have intrinsically transient nature, and the assumption of ionization equilibrium commonly used in the analysis should be critically examined.

Time-dependent collisonal-radiative model is to be developed to analyse the data taken by EIS, and to diagnose temperatures and densities of those plasmas in the outer atmospheres of the sun. No systematic models yet exist for iron ions of L- and M-shells and their transitions, which are very important for coronal plasma diagnostics. Atomic data [6] for iron ions of FeX to FeXIII are surveyed and evaluated, and most recommended data are determined. Parameters for analytical fitting functions are obtained and provided.

[1] J.L. Culhane *et al.*, Solar Physics in press (2006).
[2] J. Lang *et al.*, Appl. Optics, **45**, No.34, 8689 (2006).
[3] C.M. Korendyke *et al.*, Appl. Optics, **45**, No.34, 86 74 (2006).
[4] E. Landi *et al.*, Astrophys. J. Suppl. Ser., **162**, 261 (2006).
[5] D.H. Brooks *et al.*, Astrophys. Sp. Sci., **261**, 91 (1998).
[6] NIFS-DATA95 (2006).